

The Feasibility of Coherent Energy Transfer in Microtubules

Travis John Adrian Craddock^{1,2,3}, Douglas Friesen⁴, Jonathan Mane⁴, Stuart Hameroff⁵, and Jack A. Tuszynski^{4,6}

¹Center for Psychological Studies, Nova Southeastern University, Ft. Lauderdale, FL, USA, 33314; ²Graduate School of Computer and Information Sciences, Nova Southeastern University, Ft. Lauderdale, FL, USA, 33314;

³Institute for Neuro-Immune Medicine, Nova Southeastern University, Ft. Lauderdale, FL, USA, 33328;

⁴Department of Oncology, University of Alberta, Cross Cancer Institute, Edmonton, AB, Canada, T6G 1Z2;

⁵Departments of Anesthesiology and Psychology, Center for Consciousness Studies, The University of Arizona Health Sciences Center, Tucson, AZ, USA, 210202; Department of Physics, University of Alberta, Edmonton, AB, Canada, T6G 2E1

Communicated by Travis Craddock, Center for Psychological Studies, Graduate School of Computer and Information Sciences, Institute for Neuro-Immune Medicine, Nova Southeastern University, 3440 South University Drive, Fort Lauderdale, Florida, United States of America, 33328, +1-954-262-2868, traddock@nova.edu

Abstract

It was once purported that biological systems were far too “warm and wet” to support quantum phenomena mainly due to thermal effects disrupting quantum coherence. However recent experimental results and theoretical analyses have shown that thermal energy may assist, rather than disrupt, quantum coherence, especially in the “dry” hydrophobic interiors of biomolecules. Specifically, evidence has been accumulating for the necessary involvement of quantum coherence and entanglement between uniquely arranged chromophores in light harvesting photosynthetic complexes. Amazingly, the ‘tubulin’ subunit proteins, which comprise microtubules, also possess a distinct architecture of chromophores, namely aromatic amino acids including tryptophan. The geometry and dipolar properties of these aromatics are similar to those found in photosynthetic units indicating that tubulin may support coherent energy transfer. Tubulin aggregated into microtubule geometric lattices may support such energy transfer, which could be of import for biological signaling and communication essential to living processes. Here we perform a computational investigation of energy transfer between chromophoric amino acids in tubulin via dipole excitations coupled to the surrounding thermal environment. We present the spatial structure and energetic properties of the tryptophan residues in the microtubule constituent protein tubulin. Plausibility arguments for the conditions favoring a quantum mechanism of signal propagation along a microtubule are provided. Overall we find that coherent energy transfer in tubulin and microtubules is biologically feasible.

Keywords: energy transfer | quantum biology | optical spectra | microtubule | structure-based simulation

Introduction

Since Schrodinger asked “What is Life?” (1) a possible link between the “weird” world of quantum phenomena and biology has been hypothesized. It has been often argued that living systems are too “warm, and wet” to support quantum effects, however recent cutting edge research suggests this is not necessarily always the case. From quantum coherence in photosynthesis and magnetoreception in birds to quantum olfaction (2) and individual photon effects in vision (3), the field of quantum biology is leaping into the mainstream. This leads us to inquire, where else might the effects of quantum biology be found?

Without a doubt, the standard bearer for the emergence of quantum biology has been the coherence found in the light harvesting antennae utilized in photosynthesis. In

2007 Greg Engel et al. directly observed quantum oscillations caused by electronic coherence at 77 K in the Fenna-Matthews-Olsen (FMO) photosynthetic light harvesting complex (LHC), a temperature pushing the “warm” limit for quantum processes, catapulting this field into the spotlight (4). This limit was further pushed to an astounding 277 K, nearing physiological temperature, and effectively ruling out the “warm and wet” limit for quantum phenomena in biology (5). Furthermore, these coherent effects do not seem to be restricted to the FMO complex alone, and have been shown for LHCs in plants (LHCII) (6-8), bacteria (LH2) (9,10) and phycobiliproteins (11,12).

The theoretical basis of this coherent energy transfer is the photo-induced interaction of transition dipoles in chlorophyll molecules. The unique chromophoric nature of chlorophyll and the elegant geometrical arrangement of these pigments in the light harvesting complexes of plants

Table 1: Site and Interaction Energies in Units of cm^{-1} (Diagonal, shown in bold, are with respect to $35,688 \text{ cm}^{-1}$).

Trp	1	2	3	4	5	6	7	8
1	+1	0	-13	0	-2	-1	5	-1
2	0	+388	-41	4	1	1	-4	1
3	-13	-41	+342	2	0	1	-6	1
4	0	4	2	+207	-4	6	-59	-1
5	-2	1	0	-4	+57	21	2	11
6	-1	1	1	6	21	+102	5	-51
7	5	-4	-6	-59	2	5	+248	3
8	-1	1	1	-1	11	-51	3	0

This is consistent with previous estimates of Förster dipole-dipole energy transfer between Trps in tubulin (19)*. However, accounting for electrostatic screening effects of the medium as well as local inhomogeneous field effects yields different results depending on the dielectric constant chosen. As the dielectric constant value increases between 2 and 8.41 the coupling strengths become increasingly non-negligible.

It must be noted here that using a dielectric constant value above 4 with the screening factor $f = \epsilon_{\text{opt}}^{-1}[(\epsilon_{\text{opt}}+2)/3]^2$ yields $f > 1$. While this seems somewhat paradoxical in terms of a screening factor enhancing coupling, we consider it in the quantum viewpoint of Knox and van Amerongen (28) as the effect of the protein environment on the Trp dipole strengths. For the experimentally measured optical dielectric constant, coupling strengths up to 60 cm^{-1} are found with the most significant couplings being between Trps 2 and 3, Trps 4 and 7, and Trps 6 and 8. All coupling strengths for the dielectric constant of 8.41 are shown in Fig. 1C which accounts for the geometrical arrangement in place.

Calculated site energies using a dielectric constant value of 8.41 range between $35,888$ and $36,276 \text{ cm}^{-1}$, giving the maximum energy difference between Trps of 388 cm^{-1} . These site energies are shown in Fig. 1C and Table 1. Diagonalization of the Hamiltonian matrix (Table 2) revealed that the degree of delocalization of excited state energies is relatively small. Only for the exciton states at $36,054$, $36,176$ and $36,300 \text{ cm}^{-1}$ is there a significant delocalization over more than one pigment, with meaningful contributions between Trps 4 and 7, and Trps 2 and 3, due to the close site energies between these pigments and their relatively large couplings.

While the coupling strengths become increasingly non-negligible as the dielectric constant value increases above 2, the general line shape of the simulated spectra does not align well with experiment for values of 2 and 4.

* This study also calculates negligible intramolecular Trp-Trp energy transfer efficiencies in tubulin, however these are based on an estimated dielectric constant of 2 and an assumed spectral overlap integral for NATA in THAM buffer at pH 7.8. As Trp is highly sensitive to its local environment (76) these results are seemingly inaccurate as the calculation does not accurately reflect the protein environment.

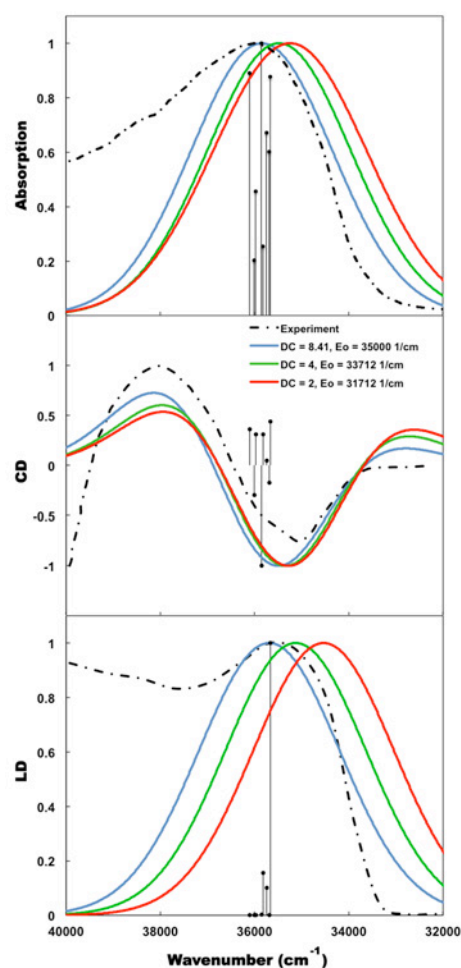


Fig. 2: Alignment of calculated spectra with experiment. Experimental spectra, bare calculated stick spectra for DC 8.41, and calculated spectra with Gaussian broadening applied for the Absorption, Circular Dichroism (CD) and Linear Dichroism (LD) of tubulin at 300 K. All values are plotted in arbitrary units similar to Vulto et al. (77).

This is most prominently seen in the CD spectra, and is not accounted for by simple shifts in E_0 alone (Fig. 2). However, when the experimentally measured optical dielectric value of tubulin is used the simulated spectra align well with experiment (see Fig. 2). This supports the use of the experimentally measured dielectric value over values between 2 and 4.

Table 2: Excited-State Energies (cm^{-1}), and Coefficients of the Eigenvectors Resulting from Diagonalization of the Hamiltonian in Table 1. Coefficients larger than 50% are shown in bold.

energies	Contribution of Trp no.							
	1	2	3	4	5	6	7	8
35663	0.04	0.00	0.00	-0.02	-0.22	0.40	-0.02	0.89
35688	-1.00	0.00	-0.04	0.01	-0.05	0.01	0.02	0.02
35746	-0.04	0.00	0.00	0.03	0.95	-0.12	0.00	0.28
35814	0.01	0.00	0.00	0.12	-0.22	-0.90	0.09	0.35
35854	0.02	0.00	0.01	0.81	0.01	0.15	0.57	-0.04
35976	0.00	-0.14	-0.21	0.56	-0.02	0.00	-0.79	-0.01
36008	0.04	-0.48	-0.84	-0.14	0.00	0.00	0.21	0.00
36100	-0.02	-0.86	0.50	-0.01	0.00	0.00	0.00	0.00

Population dynamics calculations from the Haken-Strobl (31) method were applied to the Hamiltonian in Table 1 for initial excitations occurring on each of the 8 Trp residues (see Fig. 3). It was determined that coherent beatings last for ~ 600 fs with a pure dephasing rate of 50 cm^{-1} , when the excitation starts at Trps 2, 3, 4 or 7, and for < 300 fs when starting at Trp 6 or 8. Excitations starting at Trp 1 or 5 did not produce any beating effects. When starting at Trp 2 or 3 the excitation can be seen to spread to Trp 4 and 7 reaching close to the equal population distribution of 0.125 within ~ 2 ps. Negligible exciton populations in the remaining Trps are observed in this time frame. When starting at Trp 4 or 7, the same effect is observed for Trps 2 and 3 with additional increases in exciton population for Trps 5, 6, and 8 to ~ 0.06 , spreading over the entire dimer.

Starting from the highest energy state the excitation travels from Trp 2 \rightarrow 3 \rightarrow 7 \rightarrow 4 \rightarrow 6 \rightarrow 8 covering the length of the tubulin dimer. Stacking tubulin dimers end to end in a microtubule would most likely alter this energy landscape, however it is feasible that such an arrangement could effectively transfer energy along the protofilament length as the inter-dimer spacing of Trps is uninterrupted (Fig. 4). Additionally, the unique cylindrical lattice symmetries found in the tubulin lattices of microtubules may effectively serve to enhance transfer rates and distances, and potentially enable energy transfer along helical pathways. Generalized Förster effects (32), induced by geometrical symmetries, can enhance the exciton diffusion length along cylindrically symmetric structures (33), similar to the helical arrangement of tubulin, and its chromophores, in microtubules.

Is this effect unique to tubulin and microtubules? Trp is an ubiquitous amino acid found in most all proteins in low abundance, and FRET between Trp residues and other fluorophores is a technique commonly used to probe protein structure and dynamics. In most cases this RET is restricted to a single isolated protein, or between two adjacent interacting proteins or molecules. Crystallized globular proteins have the potential to efficiently transfer

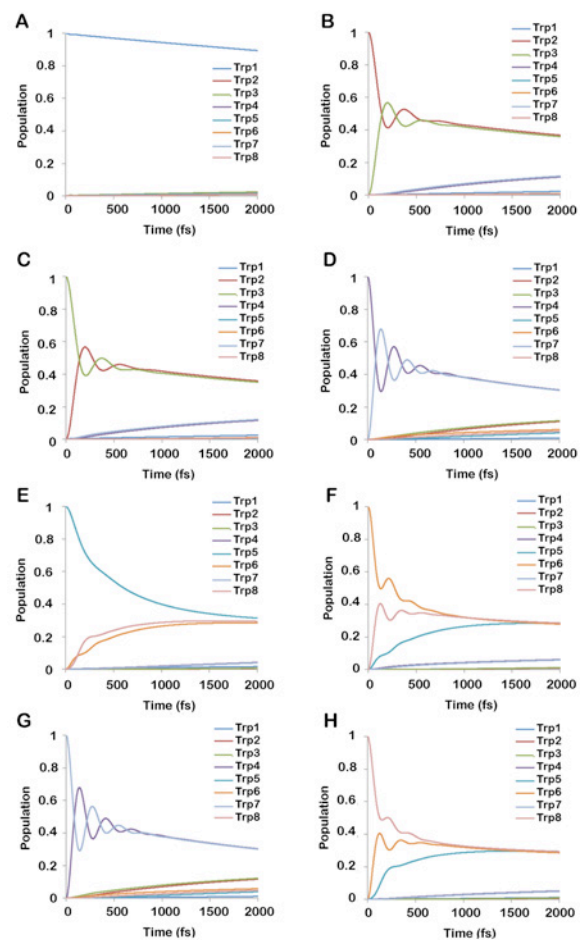


Fig. 3: Time evolution of the exciton population of each tryptophan in tubulin via the Haken-Strobl-Reineker model. Initial pure states are set as (A) Trp1: α W21, (B) Trp2: α W346, (C) Trp3: α W388, (D) Trp4: α W407, (E) Trp5: β W21, (F) Trp6: β W101, (G) Trp7: β W344 and (H) Trp8: β W397.

energy between Trp residues (34), yet these are rarely, if ever, found in biology. Protein polymers, such as the cell cytoskeleton, on the other hand are pervasive in biology, offering candidate structures for this type of energy transmission. While crystal structures for the majority of cytoskeletal components do not currently exist, comparison of their amino acid sequences reveals that the

majority of intermediate filaments have a Trp abundance less than a third of that found in tubulin (Table 3) suggesting unfavorable conditions for RET. Only actin and synemin possess comparable densities, suggesting that polymers of these molecules could support RET similar to that in tubulin and microtubules. Although the crystal structure of actin is available and reveals 4 Trp per subunit with intramolecular separations ranging between 10 and 23 Å, the intermolecular distances between these Trp clusters is > 40 Å (Fig. 4) suggesting unfavorable conditions for RET within a microfilament.

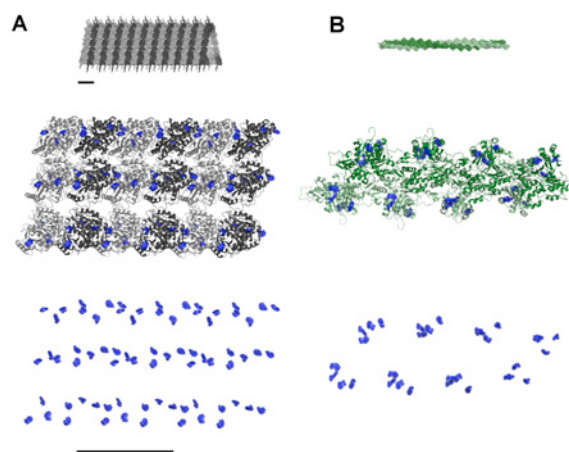


Fig. 4: Tryptophan architectures in cytoskeletal filaments. (A) Tubulin based microtubule. (B) Actin based microfilament. Scale bars are approximately 10 nm. Actin microfilaments are built using PDB ID: 2ZWH using the Oda et al. filament model (78).

Whether this has a biological role remains open. Such rapid signaling through Trp conduction pathways may coordinate the complex organization of the microtubule cytoskeleton required for the tasks of cell division, motor protein trafficking, and motility. Microtubules have been shown to reorganize in a dose-dependent manner after exposure to UV light (35-38), with the greatest effect being observed around 280 nm (38). Feasible mechanisms for these changes include the reduction of disulfide or peptide bonds induced by photoexcitation of tryptophan groups (39-42), or subtle protein structural changes due to photoinduced alterations in Trp flexibility (42). Such a signaling mechanism may explain observed the apparent UV mediated cell-to-cell influence on cell division (43). Only further investigation, both theoretically and experimentally, will tell.

Thus, we conclude that, based on this initial analysis, the unique Trp network within an individual tubulin dimer can possess significant dipolar couplings capable of supporting quantum coherent beating effects similar to those observed in the FMO photosynthetic complex (4,5), LHCII (7,8), LH2 (9,10) and phycobiliprotein LHCs (11,12). Furthermore, our results suggest that this network may support coherent energy transfer at

Table 3: Tryptophan abundance in cytoskeletal constituent molecules

Cytoskeletal Molecule	Total Residues	Trps	Trp Abundance
Tubulin monomer	~450	4	0.9%
Actin	375	4	1.1%
α -Internexin	499	1	0.2%
Desmin	470	1	0.2%
GFAP	432	1	0.2%
Keratin	564	2	0.3%
Neurofilament	916	3	0.3%
Peripherin	470	1	0.2%
Syncoilin	482	0	0.0%
Synemin	1565	15	1.0%
Vimentin	466	1	0.2%

physiological temperature between clusters of Trps in tubulin, and microtubule structures. One of the main objectives of this paper is to stimulate future experimental work in this area. While this is purely a computational prediction it supports the continued investigation of coherent energy transfer mechanisms in tubulin and microtubule lattices. Our predictions are experimentally feasible to verify employing the same methods as those used in the case of photosynthetic complexes.

Methods

Here, we give a brief summary of the computational procedures yielding site energies, excitonic couplings, optical spectra, and time evolution of exciton populations. All data will be made available on request.

Molecular Dynamics Simulation/Dominant Tryptophan Confirmation: MD Simulations were performed based on previous methods (44,45), using NAMD (46). Coordinates for the $\alpha\beta$ -tubulin dimer at 3.5 Å, GDP, GTP, and magnesium ion are from the Brookhaven National Laboratory Protein Data Bank (47) entry 1JFF (48), and PDB2PQR 1.7 (49) was used to generate per-atom charge and radius, at pH 7.0 using PROPKA (50,51), and the AMBER (52) force field. Swiss-PdbViewer 4.0 (53) was used to model the missing residues in the crystal structure (α -tubulin: 1, 35-60, 440-451, β -tubulin: 1, 438-455). GDP and GTP were modelled for use by the AMBER 94/99 force field by Meagher et al. (54). PTRAJ, using the AMBER99SB force field (55) from AMBER 10 (52) was used to neutralize the system, add counterions to reproduce physiological ionic concentrations, and add a TIP3P water cube buffer of 25 Å (63283 molecules of water). After minimization and heating to 310 K, equilibration occurred for 519 picoseconds (ps) while gradually releasing constraints on backbone atoms. Then, using periodic boundary conditions, a 17 nanosecond (ns) simulation occurred where atomic co-ordinates were saved from the trajectory every 2 ps.

PTRAJ was used to analyze the 17 ns trajectory for root mean square deviation (RMSD) of the backbone of non c-terminus residues of both alpha and beta tubulin, as well as the beta-factor of all residues. The RMSD was found to stabilize after approximately 8 ns. The final 8 ns of the total trajectory was chosen for further analysis. The GROMACS program `g_cluster` (56) was used to cluster the Trp atom positions of all frames via single linkage with a cutoff of 0.5 Å. The middle structure of the largest cluster was taken as the dominant conformation for the Trp residues.

Vertical excitation energies for Tryptophan /Site Energy Calculations: Site energies were derived from structure-based calculations of the free energy change of the protein-pigment complex (PPC) that occurs when the ground-state charge density of Trp *m* is shifted to the first excited state, analogous to methods used for the FMO complex (26,57,58).

Quantum chemical calculations of the pigments *in vacuo*, yield the charge distributions of the S_0 and $1L_a$ states and a contribution ΔE_{qm} to the $S_0 \rightarrow 1L_a$ transition energy due to the differing orientations of the Trps. Trp side chains were each isolated from the dominant conformation (described above) and capped with a hydrogen atom to complete the valence. *Ab initio* geometry optimizations at the ground state were performed using density functional theory (DFT) at the B3LYP/6-311G(d,p) (59) level. Quantum chemical calculations of the 8 lowest singly excited vertical excitation energies of Trp were done using time-dependent density functional theory (TDDFT) (60,61) at the B3LYP/6-311+G(d,p) (59) level. All calculations were performed using ORCA v2.8 (<http://cec.mpg.de/forum/>).

The vertical transition energies for the $1L_a$ state of the Trp side chains were found to be comparable to previous work using similar methods (62), however like these results our values were found to be lower than experimentally determined values (62,63). To align with experiment (38473 cm^{-1}) a scaling factor of 1.02 was applied to the calculated values. The relative quantum correction, ΔE_{qm} , to the site energy was taken as the difference between the scaled and the experimental values.

The second part of the site energy calculation results in a contribution ΔE_{coul} due to classical electrostatic interaction between the charge distributions of the S_0 and $1L_a$ states with the protein environment. Using the Charge Density Coupling (CDC) (57,58) method the site energy shift of the m^{th} Trp is calculated from the Coulomb interaction of the difference of the S_0 and $1L_a$ state partial charges $\Delta q_i^{(m)}$, obtained from the Löwdin atomic point charges in the above quantum chemical calculations, with the remaining background charges of the protein $q_j^{(bg)}$. As there can be large uncertainties when representing the Trp ring charge distribution as Löwdin atomic point charges, we have

chosen to empirically scale the charges by a factor of 0.80 to improve alignment with the experimental spectra (described below). The electrochromic shift ΔE_{coul} is given as,

$$\Delta E_{coul} = \frac{1}{\epsilon} \sum_{i=1}^N \sum_{j=1}^K \frac{\Delta q_i^{(m)} \cdot q_j^{(bg)}}{|r_i^{(m)} - r_j^{(bg)}|}$$

where N is the number of partial charges of the m^{th} Trp side chain, K is the total number of background partial charges (including other Trp residues), and $|r_i^{(m)} - r_j^{(bg)}|$ is the distance between the i^{th} difference partial charge of the m^{th} pigment and the j^{th} partial charge of the background. Background charges were taken from the AMBER99SB force field (55). Here we use the measured high frequency dielectric for tubulin setting $\epsilon = 8.41$ (30).

The site energy for the m^{th} Trp is thus given as,

$$E_m = E_0 + \Delta E_{qm} + \Delta E_{coul}$$

where E_0 is taken as 35000 cm^{-1} (285 nm) to align with experimental spectra (described below).

Excitonic Coupling Interactions: Excitonic couplings are calculated using the Point-Dipole (PD) Approximation, valid as the distance between pigments is large compared to the extension of their transition densities. The PD excitonic coupling is given as,

$$V_{mn} = f \frac{\mu_{vac}^2}{R_{mn}^3} [\vec{e}_m \cdot \vec{e}_n - 3(\vec{e}_m \cdot \vec{e}_{mn})(\vec{e}_n \cdot \vec{e}_{mn})]$$

where \vec{e}_m is a unit vector along the transition dipole moment of the m^{th} Trp, the unit vector \vec{e}_{mn} is oriented along the line connecting the centers of Trps m and n , μ_{vac} is the transition dipole moment of the $1L_a$ transition of Trp in vacuum, and the factor f effectively takes into account local field and screening effects in an effective way. In the simplest approximation due to Förster, $f = 1/\epsilon_{opt}$, accounting only for screening effects. However, when screening effects of the medium as well as local field effects are included, this becomes $f = \epsilon_{opt}^{-1}[(\epsilon_{opt}+2)/3]^2$ (64-67). Here we consider both these cases. The optical dielectric constant for a typical protein environment is given in the range of 2 – 4, however, tubulin's high frequency dielectric coefficient has been measured as 8.41 (30). For comparison, we consider the two extremes of 2 and 8.41.

Alignment with experimental spectra: The tight-binding Hamiltonian for an interacting N -body system in the presence of a single excitation is given by (68),

$$H_s = \sum_{m=1}^N \varepsilon_m |m\rangle\langle m| + \sum_{m<n}^N V_{mn} (|m\rangle\langle n| + |n\rangle\langle m|)$$

where the states $|m\rangle$ denote the excitation being at site m .

The site energies and coupling terms are given by ε_m and V_{mn} , respectively, and are calculated as described above. Exciton stick spectra for absorption, circular dichroism (CD) and linear dichroism (LD) were calculated from the orientations of the Trp molecules in the dominant confirmation and the diagonalized Hamiltonian matrix using the formula described by Pearlstein (69). Experimental spectra were calculated by applying a Gaussian function to each exciton transition using an assumed full-width half maximum value of $3,500 \text{ cm}^{-1}$ as commonly observed for Trp (70,71). These were then compared to experimental absorption, CD, and LD spectra adapted from Mozzo-Villarias et al. (72), Clark et al. (73), and Marrington et al. (74), respectively.

Exciton Population Dynamics: Time evolution of the exciton population in the Trp network in the presence of thermal fluctuations of the environment is modeled using the Haken and Strobl model (31). Here it is assumed that thermal fluctuations of the environment couple to the Trps by an electron-phonon interaction, acting only on the diagonal elements of the Hamiltonian system H_s , with the fluctuations being unbiased, uncorrelated and Gaussian in nature. Under these assumptions the Haken-Strobl equation for the density operator ρ in the Schrödinger picture is given as,

$$\dot{\rho}(t) = -\frac{i}{\hbar} [H_s, \rho(t)] + L_\phi(\rho(t))$$

where the pure-dephasing Lindblad operator is given by,

$$L_\phi(\rho(t)) = \sum_{m=1}^N \gamma_m \left[A_m \rho(t) A_m^\dagger - \frac{1}{2} A_m A_m^\dagger \rho(t) - \frac{1}{2} \rho(t) A_m A_m^\dagger \right]$$

with A_m and A_m^\dagger being the creation and annihilation operators, and γ_m the pure dephasing rates for the m^{th} Trp. As a reasonable assumption here we take γ_m to be 50 cm^{-1} for all sites. All population dynamics were computed using QuTip 2 (75).

Acknowledgements

Thanks to Dr. Chih-Yuan Tseng at Sinoveda Canada Inc. for his assistance in repairing the missing residues of the 1JFF crystal structure of the tubulin dimer, Dr. J. Robert Johansson at the RIKEN, Advanced Science Institute for his help with the QuTip programming package, and Dr. David Sept at the University of Michigan for supplying files for the actin and microfilament structures. This research has been enabled by the use of computing

resources provided by WestGrid and Compute/Calcul Canada.

References

- Schrödinger E (1944) What Is Life? The Physical Aspect of the Living Cell. (Cambridge University Press, Cambridge), p. 194.
- Lambert N, Chen YN, Cheng YC, Li CM, Chen GY, et al. (2012). Quantum biology. *Nature Physics* 9(1): 10-18.
- Fleming GR, Scholes GD, Cheng YC (2011) Quantum effects in biology. *Proc Chem* 3(1) : 38-57.
- Engel GS, Calhoun TR, Read EL, Ahn TK, Mančal T, et al. (2007) Evidence for wavelike energy transfer through quantum coherence in photosynthetic systems. *Nature* 446(7137): 782-786.
- Panitchayangkoon G, Hayes D, Fransted KA, Caram JR, Harel E, et al. (2010) Long-lived quantum coherence in photosynthetic complexes at physiological temperature. *Proc Natl Acad Sci USA* 107(29): 12766-12770.
- Schlaue-Cohen GS, Ishizaki A, Calhoun TR, Ginsberg NS, Ballottari M, et al. (2012) Elucidation of the timescales and origins of quantum electronic coherence in LHCII. *Nat Chem* 4(5): 389-395.
- Calhoun TR, Ginsberg NS, Schlaue-Cohen GS, Cheng YC, Ballottari M, et al. (2009) Quantum coherence enabled determination of the energy landscape in light-harvesting complex II. *J Phys Chem B* 113: 16291-16295.
- Schlaue-Cohen GS, Calhoun TR, Ginsberg NS, Read EL, Ballottari M, et al. (2009) Pathways of energy flow in LHCII from two-dimensional electronic spectroscopy. *J Phys Chem B* 113: 15352-15363.
- Harel E, Engel GS (2012) Quantum coherence spectroscopy reveals complex dynamics in bacterial light-harvesting complex 2 (LH2). *Proc Natl Acad Sci* 109: 706-711.
- Ostroumov EE, Mulvaney RM, Cogdell RJ, Scholes GD (2013) Broadband 2D electronic spectroscopy reveals a carotenoid dark state in purple bacteria. *Science* 340: 52-56.
- Collini E, Wong CY, Wilk KE, Curmi PM, Brumer P, et al. (2010). Coherently wired light-harvesting in photosynthetic marine algae at ambient temperature. *Nature* 463(7281): 644-647.
- Turner DB, Dinshaw R, Lee KK, Belsle M, Wilk KE, et al. (2012) Quantitative investigations of quantum coherence for a light-harvesting protein at conditions simulating photosynthesis. *Phys Chem Chem Phys* 14: 4857-4874.
- Strümpfer J, Şener M, Schulten K (2012) How Quantum Coherence Assists Photosynthetic Light-Harvesting *J Phys Chem Lett* 3(4): 536-542.
- Forster T (1948) Excitation transfer. *Ann Phys* 2: 12-19.
- Andrews DL, Curutchet C, Scholes GD (2011) Resonance energy transfer: beyond the limits. *Laser Photon Rev* 5(1): 114-123.
- Beljonne D, Curutchet C, Scholes GD, Silbey RJ (2009) Beyond Förster resonance energy transfer in biological and nanoscale systems. *J Phys Chem B* 113(19): 6583-6599.
- Würthner F, Kaiser TE, Saha-Möller CR (2011) J-Aggregates: From Serendipitous Discovery to Supramolecular Engineering of Functional Dye Materials. *Angew Chem Int Ed* 50: 3376-3410.
- Saikin SK, Eisfeld A, Valleeau S, Aspuru-Guzik A (2013) Photonics meets excitonics: natural and artificial molecular aggregates. *Nanophotonics* 2(1): 21-38.
- Sardar PS, Maity SS, Das L, Ghosh S (2007) Luminescence Studies of Perturbation of Tryptophan Residues of Tubulin in the Complexes of Tubulin with Colchicine and Colchicine Analogues. *Biochem* 46: 14544-14556.
- Monshouwer R, Abrahamsson M, van Mourik F, van Grondelle R (1997) Superradiance and exciton delocalization in bacterial photosynthetic light-harvesting systems. *J Phys Chem B* 101(37): 7241-7248.
- Guha S, Rawat SS, Chattopadhyay A, Bhattacharyya B (1996) Tubulin Conformation and Dynamics: A Red Edge Excitation Shift Study. *Biochem* 35(41): 13426-13433.
- Weber G, Shinitzky M (1970) Failure of Energy Transfer between Identical Aromatic Molecules on Excitation at the Long Wave Edge of the Absorption Spectrum. *Proc Natl Acad Sci* 65(4): 823-830

23. Hameroff S, Nip A, Porter M, Tuszynski J (2002) Conduction pathways in microtubules, biological quantum computation, and consciousness. *Biosystems* 64(1-3): 149-168.
24. Hayes D, Griffin BG, Engel GS (2013) Engineering Coherence Among Excited States in Synthetic Heterodimer Systems. *Science* 340(6139): 1431-1434.
25. Shim S, Rebentrost P, Valleau S, Aspuru-Guzik A (2012) Atomistic Study of the Long-Lived Quantum Coherences in the Fenna-Matthews-Olson Complex. *Biophys J* 102(3): 649-660.
26. Müh F, Madjet MEA, Adolphs J, Abdurahman A, Rabenstein B, et al. (2007) α -Helices direct excitation energy flow in the Fenna-Matthews-Olson protein. *Proc Natl Acad Sci USA* 104(43): 16862-16867.
27. Huh J, Saikin SK, Brookes JC, Valleau S, Fujita T, et al. (2014) Atomistic Study of Energy Funneling in the Light-Harvesting Complex of Green Sulfur Bacteria. *J Amer Chem Soc* 136(5): 2048-2057.
28. Knox RS, van Amerongen H (2002) Refractive Index Dependence of the Förster Resonance Excitation Transfer Rate. *J Phys Chem B* 106(20): 5289-5293.
29. García-Moreno BE, Dwyer JJ, Gittis AG, Lattman EE, Spencer DS, et al. (1997) Experimental measurement of the effective dielectric in the hydrophobic core of a protein. *Biophys Chem* 64(1-3): 211-224.
30. Mershin A, Kolomenski AA, Schuessler HA, Nanopoulos DV (2004) Tubulin dipole moment, dielectric constant and quantum behavior: computer simulations, experimental results and suggestions. *Biosystems* 77(1-3): 73-85.
31. Haken H, Strobl G (1973). An exactly solvable model for coherent and incoherent exciton motion. *Zeitschrift für Physik* 262(2): 135-148.
32. Scholes GD, Jordanides XJ, Fleming GR (2001) Adapting the Förster Theory of Energy Transfer for Modeling Dynamics in Aggregated Molecular Assemblies. *J Phys Chem B* 105(8): 1640-1651.
33. Abasto DF, Mohseni M, Lloyd S, Zanardi P (2012) Exciton diffusion length in complex quantum systems: the effects of disorder and environmental fluctuations on symmetry-enhanced supertransfer. *Phil Trans R Soc A* 370: 3750-3770.
34. Desie G, Boens N, De Schryver FC (1986) Study of the time-resolved tryptophan fluorescence of crystalline alpha-chymotrypsin. *Biochem* 25(25): 8301-8308.
35. Krasylenko Y, Yemets A, Blume Y (2013) Plant microtubules reorganization under the indirect UV-B exposure and during UV-B-induced programmed cell death. *Plant Signal Behav* 8(5): e24031
36. Staxén I, Bergounioux C, Bormann JF (1993) Effect of ultraviolet radiation on cell division and microtubule organization in *Petunia hybrida* protoplasts. *Protoplasma* 173(1-2): 70-76.
37. Zamansky GB, Chou IN (1987) Environmental wavelengths of ultraviolet light induce cytoskeletal damage. *J Invest Dermatol* 89(6): 603-606.
38. Zaremba TG, LeBon TR, Millar DB, Smejkal RM, Hawley RJ (1984) Effects of ultraviolet light on the in vitro assembly of microtubules. *Biochemistry* 23(6): 1073-1080
39. Neves-Petersen MT et al. (2002) High probability of disrupting a disulphide bridge mediated by an endogenous excited tryptophan residue. *Protein Sci* 11(3): 588-600.
40. Vanhooren A, Devreese B, Vanhee K, Van Beeumen J, Hanssens I (2002) Photoexcitation of tryptophan groups induces reduction of two disulfide bonds in goat α -lactalbumin. *Biochem* 41(36): 11035-11043.
41. Wu LZ, Sheng YB, Xie JB, Wang W (2008) Photoexcitation of tryptophan groups induced reduction of disulfide bonds in hen egg white lysozyme. *J Mol Struct* 882(1): 101-106.
42. Weisenborn P, Meder H, Egmond MR, Visser TJ, van Hoek A (1996) Photophysics of the single tryptophan residue in *Fusarium solani* Cutinase: Evidence for the occurrence of conformational substates with unusual fluorescence behaviour. *Biophys Chem* 58(3): 281-288.
43. Fels D (2009) Cellular Communication through Light. *PLoS ONE* 4(4): e5086.
44. Barakat K, Mane J, Friesen D, Tuszynski J. (2010) Ensemble-based virtual screening reveals dual-inhibitors for the p53-MDM2/MDMX interactions. *J Mol Graph Model* 28: 555-568.
45. Friesen DE, Barakat KH, Semenchenko V, Perez-Pineiro R, Fenske BW, et al. (2012) Discovery of small molecule inhibitors that interact with γ -tubulin. *Chem Biol Drug Des* 79: 639-652.
46. Phillips JC, Braun R, Wang W, Gumbart J, Tajkhorshid E, et al. (2005) Scalable molecular dynamics with NAMD. *J Comput Chem* 26: 1781-1802.
47. Bernstein FC, Koetzle TF, Williams GJ, Meyer Jr EF, Brice MD, et al. (1977) The Protein Data Bank: A Computer-based Archival File For Macromolecular Structures. *J Mol Biol* 112: 535-542.
48. Löwe J, Li H, Downing KH, Nogales E (2001) Refined structure of $\alpha\beta$ -tubulin at 3.5 Å resolution. *J Mol Biol* 313: 1045-1057.
49. Dolinsky TJ, Nielsen JE, McCammon JA, Baker NA (2004) PDB2PQR: an automated pipeline for the setup of Poisson-Boltzmann electrostatics calculations. *Nucleic Acids Res* 32: W665-667.
50. Li H, Robertson AD, Jensen JH (2005). Very fast empirical prediction and rationalization of protein pKa values. *Proteins: Struct Funct Bioinf* 61(4): 704-721.
51. Bas DC, Rogers DM, Jensen JH (2008). Very fast prediction and rationalization of pKa values for protein-ligand complexes. *Proteins: Struct Funct Bioinf* 73(3): 765-783.
52. Case DA, Darden TA, Cheatham III TE, Simmerling CL, Wang J, et al. (2008) Amber 10 (University of California, San Francisco), p. 306.
53. Guex N, Peitsch MC (1997) SWISS-MODEL and the Swiss-PdbViewer: an environment for comparative protein modeling. *Electrophoresis* 18: 2714-2723.
54. Meagher KL, Redman LT, Carlson HA (2003) Development of polyphosphate parameters for use with the AMBER force field. *J Comput Chem* 24: 1016-1025.
55. Hornak V, Abel R, Okur A, Strockbine B, Roitberg A, et al. (2006) Comparison of multiple Amber force fields and development of improved protein backbone parameters. *Proteins* 65: 712-725.
56. Van Der Spoel D, Lindahl E, Hess B, Groenhof G, Mark AE, et al. (2005). GROMACS: fast, flexible, and free. *J Comput Chem* 26(16): 1701-1718.
57. Adolphs J, Müh F, Madjet MEA, Renger T (2008). Calculation of pigment transition energies in the FMO protein. *Photosyn Res* 95(2-3): 197-209.
58. Adolphs J, Müh F, Madjet MEA, Busch MSA, Renger T (2010). Structure-based calculations of optical spectra of photosystem I suggest an asymmetric light-harvesting process. *J Am Chem Soc* 132(10): 3331-3343.
59. Krishnan RBS, Binkley JS, Seeger R, Pople JA (1980). Self-consistent molecular orbital methods. XX. A basis set for correlated wave functions. *J Chem Phys* 72: 650.
60. Koch W, Holthausen MC (2001). *A Chemist's Guide to Density Functional Theory* (Vol. 2). (Wiley-Vch, Weinheim), p. 306.
61. Parr RG, Yang W (1989) *Density Functional Theory of Atoms and Molecules*. (Oxford University Press, New York), p. 352.
62. Rogers DM, Besley NA, O'Shea P, Hirst JD (2005) Modeling the Absorption Spectrum of Tryptophan in Proteins. *J Phys Chem B* 109: 23061-23069.
63. Serrano-Andrés L, Roos BO (1996) Theoretical Study of the Absorption and Emission Spectra of Indole in the Gas Phase and in a Solvent. *J Am Chem Soc* 118: 185-195.
64. Juzeliūnas G, Andrews DL (1994) Quantum electrodynamics of resonant energy transfer in condensed matter. *Phys Rev B* 49(13): 8751.
65. Juzeliūnas G, Andrews DL (1994) Quantum electrodynamics of resonant energy transfer in condensed matter. II. Dynamical aspects. *Phys Rev B* 50(18): 13371.
66. Mennucci B, Curutchet C (2011) The role of the environment in electronic energy transfer: a molecular modeling perspective. *Phys Chem Chem Phys* 13(24): 11538-11550.
67. Scholes GD, Fleming GR (2000) On the mechanism of light harvesting in photosynthetic purple bacteria: B800 to B850 energy transfer. *J Phys Chem B* 104(8): 1854-1868.

68. May V, Kühn O (2004) Charge and energy transfer dynamics in molecular systems, 2nd, Revised and Enlarged Edition. (Wiley-Vch., Weinheim), p. 490.
69. Pearlstein RM (1991) in Chlorophylls, ed Scheer H. (CRC press, Boca Raton), pp. 1047-1978.
70. Léonard J, Portuondo-Campa E, Cannizzo A, van Mourik F, van der Zwan G, et al. Functional electric field changes in photoactivated proteins revealed by ultrafast Stark spectroscopy of the Trp residues. *Proc Natl Acad Sci USA* 106(19): 7718-7723.
71. Schenkl S, van Mourik F, van der Zwan G, Haacke S, Chergui M (2005) Probing the ultrafast charge translocation of photoexcited retinal in bacteriorhodopsin. *Science* 309: 917-920.
72. Mozo-Villarias A, Morros A, Andreu JM (1991). Thermal transitions in the structure of tubulin. *Eur Biophys J* 19(6): 295-300.
73. Clark DC, Martin SR, Bayley PM (1981). Conformation and assembly characteristics of tubulin and microtubule protein from bovine brain. *Biochem* 20(7): 1924-1931.
74. Marrington R, Seymour M, Rodger A (2006) A new method for fibrous protein analysis illustrated by application to tubulin microtubule polymerisation and depolymerisation. *Chirality* 18(9): 680-690.
75. Johansson JR, Nation PD, Nori F (2013) QuTiP 2: A Python framework for the dynamics of open quantum systems. *Comp Phys Comm* 184: 1234.
76. Pan CP, Muiño PL, Barkley MD, Callis PR (2011) Correlation of Tryptophan Fluorescence Spectral Shifts and Lifetimes Arising Directly from Heterogeneous Environment. *J Phys Chem B* 115(12): 3245-3253
77. Vulto SI, de Baat MA, Louwe RJ, Permentier HP, Neef T, et al. (1998). Exciton simulations of optical spectra of the FMO complex from the green sulfur bacterium *Chlorobium tepidum* at 6 K. *J Phys Chem B* 102(47): 9577-9582.
78. Oda T, Iwasa M, Aihara T, Maéda Y, Narita A (2009) The nature of the globular-to fibrous-actin transition. *Nature* 457(7228): 441-445.